The North Pacific Oxygen Uptake Rates over the Past Half Century

EUN YOUNG KWON

School of Earth and Environmental Sciences (BK21), Seoul National University, Seoul, South Korea

CURTIS DEUTSCH

School of Oceanography, University of Washington, Seattle, Washington

SHANG-PING XIE

Scripps Institution of Oceanography, University of California, San Diego, La Jolla, California

SUNKE SCHMIDTKO

GEOMAR Helmholz Centre for Ocean Research Kiel, Kiel, Germany

YANG-KI CHO

School of Earth and Environmental Sciences, Research Institute of Oceanography, Seoul National University, Seoul, South Korea

(Manuscript received 28 February 2014, in final form 2 October 2015)

ABSTRACT

The transport of dissolved oxygen (O_2) from the surface ocean into the interior is a critical process sustaining aerobic life in mesopelagic ecosystems, but its rates and sensitivity to climate variations are poorly understood. Using a circulation model constrained to historical variability by assimilation of observations, the study shows that the North Pacific thermocline effectively takes up O_2 primarily by expanding the area through which O_2-rich mixed layer water is detrained into the thermocline. The outcrop area during the critical winter season varies in concert with the Pacific decadal oscillation (PDO). When the central North Pacific Ocean is in a cold phase, the winter outcrop window for the central mode water class (CMW; a neutral density range of $\gamma = 25.6$–26.6) expands southward, allowing more O_2-rich surface water to enter the ocean's interior. An increase in volume flux of water to the CMW density class is partly compensated by a reduced supply to the shallower densities of subtropical mode water ($\gamma = 24.0$–25.5). The thermocline has become better oxygenated since the 1980s partly because of strong O_2 uptake. Positive O_2 anomalies appear first near the outcrop and subsequently downstream in the subtropical gyre. In contrast to the O_2 variations within the ventilated thermocline, observed O_2 in intermediate water (density range of $\gamma = 26.7$–27.2) shows a declining trend over the past half century, a trend not explained by the open ocean water mass formation rate.

1. Introduction

Marine heterotrophs require O_2 for respiration, and O_2 variability constrains the habitat of many species over large volumes of the deep ocean (Deutsch et al. 2015; Vaquer-Sunyer and Duarte 2008). To maintain a habitable deep ocean, O_2 must be supplied via the downward transport of surface water rich in the O_2 obtained from the atmosphere and photosynthesis. An imbalance between physical input and biological consumption rates, both highly sensitive to climate, can change O_2 levels over time. Such an imbalance has been widely predicted to occur with climate warming, driven largely by reduced O_2 supply (Keeling et al. 2010). Over the past 50 years, O_2 has declined within the subpolar gyre, while it has slightly increased within the subtropics (e.g., Emerson et al. 2004; Deutsch et al. 2005; Stramma

Corresponding author address: Eun Young Kwon, School of Earth and Environmental Sciences (BK21), Seoul National University, 1 Gwanak-ro, Gwanak-gu, Seoul 151-742, South Korea.
E-mail: ekwon76@snu.ac.kr

DOI: 10.1175/JCLI-D-14-00157.1

et al. 2012). The linear trends are superimposed on more pronounced multidecadal fluctuations that may be associated with changes in ventilation rate, circulation, and/or respiration (e.g., Deutsch et al. 2005, 2006) accentuated by the decadal residence time of the thermocline circulation (Ito and Deutsch 2010). Improved understanding of the supply mechanism and its relationship to climate variations will help us better understand observed O_2 changes.

As a result of strong stratification within the North Pacific, convection is restricted to relatively shallow depths (usually <250 m; e.g., Suga et al. 2004), and the ventilation of deeper layers requires the transfer of water from the surface mixed layer into the thermocline. The transfer is primarily achieved through subduction (Sallée et al. 2012; also see below). The subduction of O_2-rich surface water occurs through both wind-driven Ekman downwelling (Huang and Qiu 1994) and the injection of winter mixed layer water beneath the shoaling mixed layer base (Stommel 1979; Williams et al. 1995). The subduction mainly occurs at the boundary between subtropical and subpolar gyres, where seasonal air–sea heat exchange and boundary layer mixing are strong (Oka et al. 2011). A recent study by Kwon et al. (2013) highlighted the importance of the winter outcrop area, where thermocline waters are exposed at the sea surface during winter, for determining the annual mean subduction of surface water to the thermocline. The seasonal detrainment of mixed layer water mainly occurs during early spring stratification (Woods and Barkmann 1986) through a large outcropping area created during winter cooling. In contrast, seasonal entrainment of thermocline water back to the mixed layer occurs gradually over a contracted outcrop window. Repeating seasonal cycles can lead to the net downward transport of water masses into the thermocline (Marshall 1997; Kwon et al. 2013).

In this paper, we show that the seasonal cycle of outcrop expansion and contraction represents an important mechanism by which the North Pacific takes up O_2 (section 2). By diagnosing the change in the O_2 transfer rate over the past half century, we show that the North Pacific's O_2 uptake rate has changed in concert with the Pacific decadal oscillation (PDO; Mantua et al. 1997), primarily through its influence on the interannual variability of the winter outcrop area (section 3). Analysis of historical hydrographic data (section 4) reveals a potential link between the multidecadal fluctuation in the estimated O_2 supply and observed O_2 variability within the North Pacific ventilated gyres. While we mainly focus on mode water density ranges that are directly ventilated from the open ocean's surface, substantial O_2 decline has been reported for density layers that do not outcrop at the open ocean surface (e.g., Ono et al. 2001; Whitney et al. 2007; Mecking et al. 2008). Thus, we briefly discuss our results in the context of reported deoxygenation (section 4c).

2. Diagnosing O_2 exchange rate

a. Background

Processes contributing to the exchange of O_2 between the surface and the interior ocean include the subduction and mixing of O_2-rich surface water across the base of the mixed layer. The area-integrated subduction rate, M, of O_2-rich mixed layer water is diagnosed by employing the kinematic approach of Cushman-Roisin (1987) as follows:

$$M(\gamma,t)=\int_{A(\gamma_1\le\gamma<\gamma_2)}[\mathrm{O_2}]_h\left(-\frac{\partial h}{\partial t}-U_h\nabla_l h-w_h\right)dA\,, \tag{1}$$

where $A(\gamma_1 \le \gamma < \gamma_2)$ is the area over which waters of density $\gamma_1 \le \gamma < \gamma_2$ outcrop at the base of the mixed layer; h is the mixed layer thickness determined using a density difference of $0.03\,\mathrm{kg\,m^{-3}}$ from the sea surface (de Boyer Montégut et al. 2004); U_h is the lateral velocity of water at the base of the mixed layer; w_h is the vertical velocity of water at the base of the mixed layer; and ∇_l is the horizontal gradient operator. A positive M indicates downward transfer and is referred to as subduction. A negative M indicates upward transfer, also known as obduction.

Combined with mixing effects, the exchange rate becomes

$$E(\gamma,t)=\int_{A(\gamma_1\le\gamma<\gamma_2)}[\mathrm{O_2}]_h\left(-\frac{\partial h}{\partial t}-U_h\nabla_l h-w_h\right)-K_l\cdot\nabla_l[\mathrm{O_2}]_h\cdot\nabla_l h-K_v\cdot\nabla_v[\mathrm{O_2}]_h\,dA\,, \tag{2}$$

where ∇_v is the vertical gradient operator; and K_l and K_v are the horizontal and vertical mixing coefficients, respectively, fixed at upper bounds of $K_l = 10^4\,\mathrm{m^2\,s^{-1}}$ and $K_v = 10^{-4}\,\mathrm{m^2\,s^{-1}}$ (Sallée et al. 2012). A lateral mixing component that is perpendicular to the base of the mixed layer is required. Hence, the lateral mixing term (i.e., $K_l\cdot\nabla_l[\mathrm{O_2}]_h\cdot\nabla_l h$) includes $\nabla_l h$.

Since we are concerned with the interannual variability of the O_2 exchange rate across the moving base of the mixed layer, we employ the instantaneous subduction rate of Cushman-Roisin (1987) rather than the time-invariant subduction rate into the main thermocline of Marshall et al. (1993). When averaged over several annual cycles, the time-averaged subduction rate of O_2 across the time-varying mixed layer base is not necessarily equal to the subduction rate across the time-invariant winter

mixed layer, because diapynal mixing within the seasonal thermocline can modulate the O_2 transfer rate into the main thermocline (Nurser et al. 1999; Marshall et al. 1999; Kwon et al. 2013). Therefore, the O_2 subduction rate obtained using Eq. (1) includes not only O_2 fluxes entering the permanent thermocline, but also O_2 fluxes subject to alteration by diapycnal mixing and remineralization within the seasonal thermocline.

b. *Attributing the mechanisms of subduction*

To elucidate the mechanism by which O_2-rich mixed layer water subducts, we decompose the net subduction rate into its constituent mechanisms using Eq. (1). The contributions are from lateral induction beneath the temporally varying mixed layer base (i.e., $Dh/Dt = \partial h/\partial t + U_h \nabla_l h$; Williams et al. 1995; Kwon et al. 2013) and the vertical transport of water (w_h) dominated by Ekman pumping/suction using the following equation:

$$M(\gamma, t) = \int_A -[\mathrm{O_2}]_h \frac{Dh}{Dt}\, dA + \int_A -[\mathrm{O_2}]_h w_h\, dA. \qquad (3)$$

The first term on the right-hand side of Eq. (3) provides the downward transport of O_2-rich surface water across the base of the mixed layer following a water parcel. Rapid shoaling of the mixed layer base during early spring can make a significant contribution to this term (Kwon et al. 2013). The second term arises from vertical movements of water mainly induced by wind stress curl (i.e., Ekman upwelling/downwelling).

To determine the contribution of each term in Eq. (1) to interannual variability, we calculate the mean seasonal cycles for the outcrop area $\overline{A}$, the time rate of change in the mixed layer depth $\partial h/\partial t$, and the terms involving ocean circulation $\overline{U_h \nabla_l h}$ and $\overline{w_h}$. Then we replace the corresponding terms in Eq. (1) with the mean seasonal cycles. Each of these three cases can be described mathematically thusly:

Constant area case: $M_A(\gamma, t)$

$$= \int_{A(\gamma_1 \le \gamma < \gamma_2)} [\mathrm{O_2}]_h \left(-\frac{\partial h}{\partial t} - U_h \nabla_l h - w_h \right) dA \qquad (4)$$

Constant mixed layer case: $M_h(\gamma, t)$

$$= \int_{A(\gamma_1 \le \gamma < \gamma_2)} [\mathrm{O_2}]_h \left(-\frac{\overline{\partial h}}{\partial t} - U_h \nabla_l h - w_h \right) dA \qquad (5)$$

Constant circulation case: $M_c(\gamma, t)$

$$= \int_{A(\gamma_1 \le \gamma < \gamma_2)} [\mathrm{O_2}]_h \left(-\frac{\partial h}{\partial t} - \overline{U_h \nabla_l h} - \overline{w_h} \right) dA, \qquad (6)$$

where the overbar represents the mean seasonal cycle of each term, averaged over the time period from 1958 to 2007. Correlations between the two subduction estimates obtained from the fully varying case and the idealized cases are then used to attribute contributions from the varying outcrop area, mixed layer depths, and circulation. The portion of variance attributed to each component is computed as the residual variance that is not explained by the time series when that component is held constant. Although these processes are not independent of one another, the method helps us understand their relative importance in determining the temporal variation of the subduction rate.

c. *The model and data*

We use the Simple Ocean Data Assimilation version 2.1.6 (SODA; Carton et al. 2000a,b; Carton and Giese 2008; available at http://www.atmos.umd.edu/~ocean/) to estimate the subduction rate of North Pacific upper-water masses. SODA uses an ocean general circulation model based on Parallel Ocean Program numerics (Smith et al. 1992). Vertical mixing of momentum, heat, and salt is represented using K-profile parameterization (Large et al. 1994). The model is run at a horizontal resolution of 0.25° × 0.4°, and model solutions of temperature, salinity, and velocity are remapped onto uniform 0.5° × 0.5° horizontal grid points (Carton and Giese 2008). The vertical resolution ranges from 10 m near the surface to ~250 m near the bottom, with a total of 40 vertical levels. The SODA hindcast simulation spans the time period from 1958 to 2007. An optimal interpolation method is used to assimilate temperature and salinity profiles and satellite sea surface temperature into the numerical model (Carton and Giese 2008). The model is known to reasonably capture observed large-scale upper-ocean physical structure and circulations (Carton et al. 2000b; Carton and Giese 2008).

In Figs. 1b, 1d, and 2, we compare some of the climatological mean features relevant to O_2 subduction between the model and the *World Ocean Atlas 2009* (*WOA09*; Locarnini et al. 2010; Antonov et al. 2010; Garcia et al. 2010). The surface distribution of winter (January–March) mean saturated O_2 concentration, estimated using temperatures and salinity, compares well between SODA and the *WOA09* (Figs. 1b and 1d). Both the model and the observations indicate that saturated O_2 concentrations increase from ~200 μmol kg^{-1} in the southern flank of the subtropical gyre to ~350 μmol kg^{-1} in the western subpolar gyre. The distribution of observed surface O_2 concentration is similar to that for saturated O_2 concentration (Fig. 1a), with a slight (<10%) supersaturation occurring within the subtropical gyre and an undersaturation occurring within the subpolar gyre (Fig. 1c). The surface distribution of winter mean

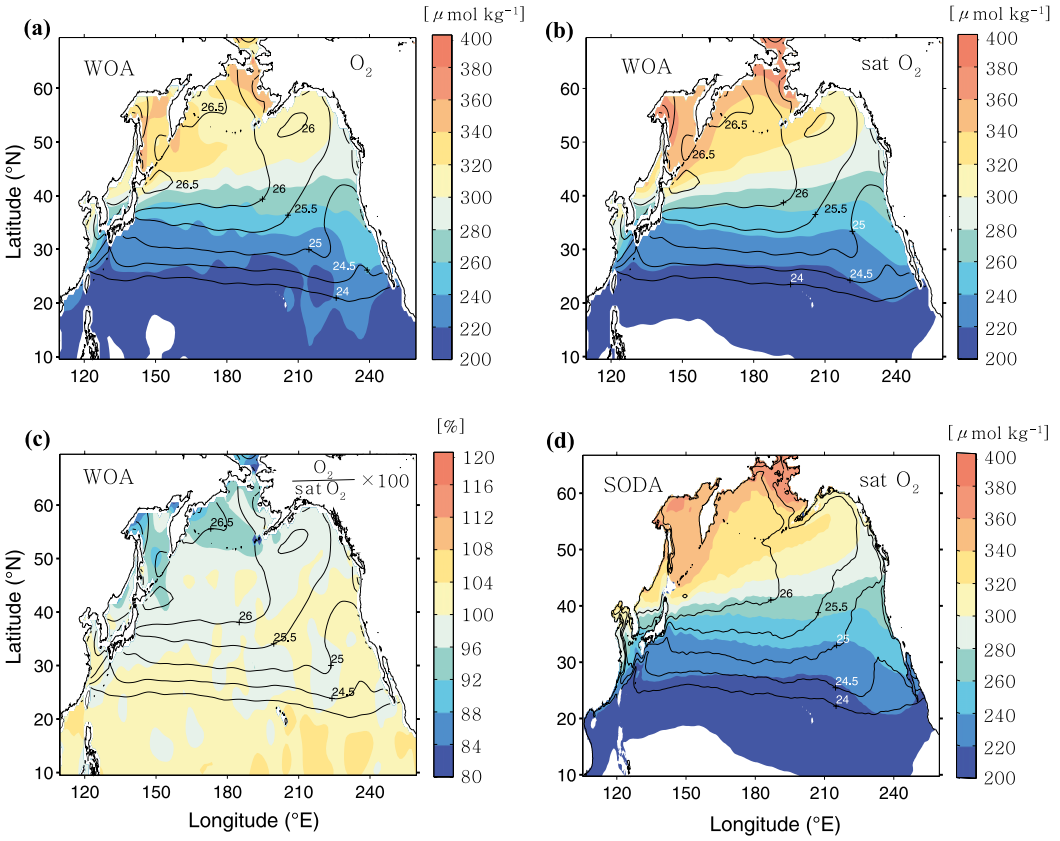

FIG. 1. Winter mean surface O_2 concentrations overlain with winter mean neutral density. (a) Colored shading indicates surface O_2 concentrations obtained from *WOA09*. Solid lines indicate the neutral density calculated using *WOA09* hydrographic data. (b) Surface saturated O_2 (sat O_2) estimated using *WOA09* hydrographic data. Contour lines as in (a). (c) Percent saturation of surface O_2, estimated from *WOA09* [i.e., (a) divided by (b) times 100]. Contour lines as in (a). (d) Surface saturated O_2 estimated from SODA temperature and salinity. Solid lines indicate the neutral density calculated using SODA. The SODA-based estimates are averaged between 1958 and 2007.

density is also well reproduced in the model, especially in the open ocean (Figs. 1c and 1d).

The winter mixed layer depth, determined using a density difference of 0.03 kg m^{-3} from the sea surface (de Boyer Montégut et al. 2004), is reasonably reproduced in the model with some notable discrepancies (Fig. 2). In both the model and observations, deep mixed layers of ~150 m form in the northwest Pacific at the transition area between the subtropical and subpolar gyres. The band of the mixed layer maxima extends from the northwest Pacific off the east coast of Japan toward the central North Pacific, coincident with mode water formation regions (Hanawa and Talley 2001; Yasuda 2003; Suga et al. 2004). Along the midlatitude northwest Pacific between 30° and 40°N, excess heat loss to the atmosphere (Fig. 3a) associated with strong winds triggers deep convection within the mixed layer during winter. Despite the qualitative agreements, the simulated winter mixed layer depths in the northeast Pacific between 40° and 50°N are shallower than the observations. Another notable discrepancy is the model's inability to capture the observed separation of two deep mixed layer bands, one located at the Oyashio Front near 40°N and the other located at the Kuroshio Front near 30°N. Instead, in the model, deep winter mixed layers form in a broad region of the northwest Pacific as shown in Fig. 2b. Since we focus on the subduction rate integrated over a broad range of density layers (see below), the model's inability to reproduce the finescale structure of the mixed layer depth likely does not undermine our conclusions.

In addition to climatological mean features, the SODA simulation is able to reasonably reproduce multidecadal climate variability. We compute the empirical orthogonal function (EOF) for deseasonalized near-surface temperature, averaged over the top 10 m. The leading EOF pattern (Fig. 4a) and the associated principal component time series (Fig. 4b) roughly agree with those of Mantua et al. (1997), who used independent datasets of sea surface temperature to define the

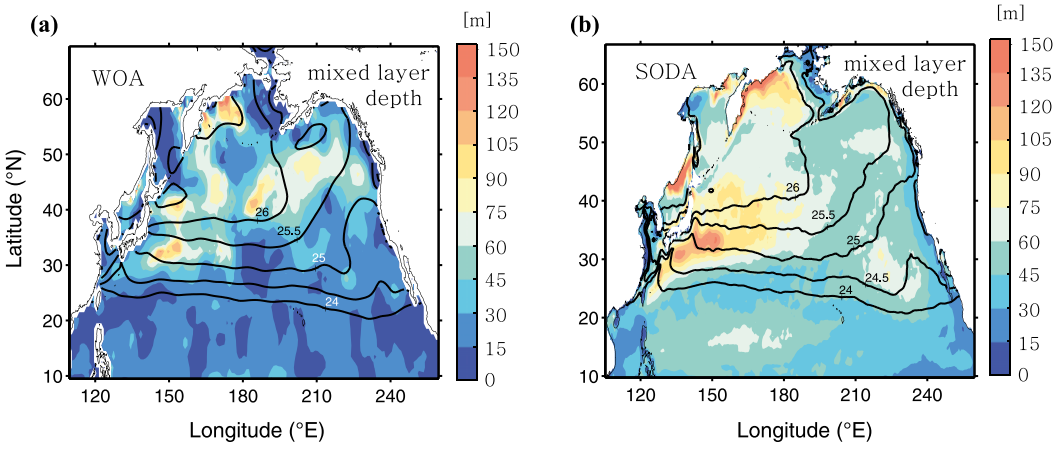

FIG. 2. Winter mean mixed layer depth determined using a density difference of 0.03 kg m^{-3} from the sea surface. (a) Estimate from *WOA09*. (b) Estimate from SODA averaged over 1958–2007. Winter mean surface neutral densities are shown as black solid lines.

PDO index. Such agreement provides confidence in the use of the SODA simulation for the study of large-scale upper-ocean processes and their decadal variability in the North Pacific.

To estimate the subduction of O_2 that is maximally consistent with both the observed distribution of O_2 and with the large-scale circulation, we combine the physical quantities from SODA with climatological O_2 fields. This approach avoids the relatively large biases present in model simulations of the O_2 cycle, which are in any case not part of the SODA model. To combine these datasets, we first obtain the monthly mean O_2 concentration at the base of the mixed layer using 1° × 1° *WOA09* monthly climatologies for temperature, salinity, and O_2 (Locarnini et al. 2010; Antonov et al. 2010; Garcia et al. 2010). The O_2 concentration interpolated to the base of the mixed layer is very close to the surface value (Fig. 1a). The vertically interpolated *WOA09* O_2 data are then linearly interpolated to 0.5° × 0.5° SODA grids. We use the interpolated monthly

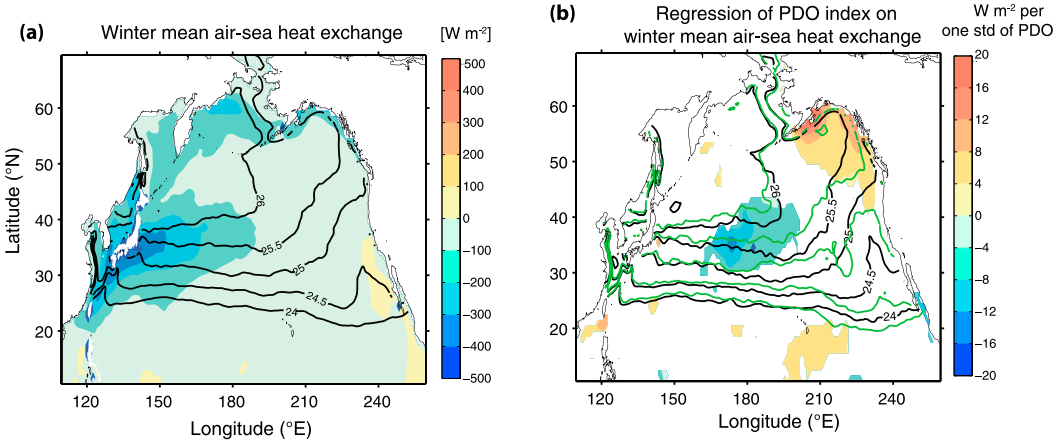

FIG. 3. Winter mean air–sea heat exchange, computed using version 2 of the Common Ocean Reference Experiment global air–sea flux dataset (Large and Yeager 2009). (a) Winter mean heat fluxes averaged over 1958–2006 (W m^{-2}). Positive values indicate heat gain by the ocean, and negative values indicate heat loss to the atmosphere. Black contour lines are the winter mean surface neutral densities averaged over 1958–2006, obtained from SODA. (b) The regression pattern of the annual mean PDO index on the annually averaged winter air–sea heat exchange (W m^{-2} per one standard deviation of the PDO index). Values significant at 95% are shown. Positive values represent anomalously increased heat inputs to the ocean (or decreased heat losses to the atmosphere) during positive PDO years, while negative values represent anomalously decreased heat inputs to the ocean (or increased heat losses to the atmosphere). Black (green) contour lines represent the winter neutral densities composited for years with the PDO index greater than one standard deviation (less than minus one standard deviation). The PDO index is obtained from Mantua et al. (1997) (available at http://jisao.washington.edu/pdo/PDO.latest).

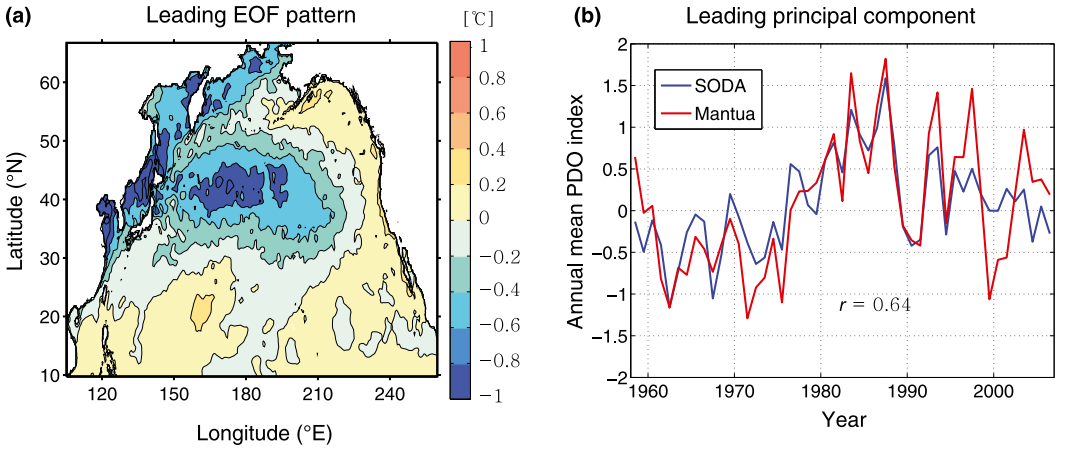

FIG. 4. The SODA representation of the PDO. (a) The leading EOF pattern of the deseasonalized monthly mean temperature at the surface layer (top 10 m), computed using SODA. (b) The blue solid line is the associated principal component time series averaged annually, as obtained from SODA. The SODA-based estimate of the PDO index (blue solid line) is compared to the PDO index (red solid line) obtained from Mantua et al (1997). The correlation coefficient between the two time series is $r = 0.64$.

mean O_2 fields repeatedly for the product of O_2 and the water mass subduction rate across the base of the mixed layer [as expressed in Eq. (1)] over the simulation period from 1958 to 2007. This approach neglects interannual variations in surface O_2. To evaluate the potential importance of surface O_2 variability, we also derive subduction rates assuming that surface O_2 is at equilibrium with the atmosphere, allowing its interannual variations to be computed from the SODA temperature and salinity. The two approaches do not make a discernible difference for interannual variations of O_2 subduction rate, because surface O_2 concentration variation plays a minor role in the interannual variability of the O_2 subduction (see section 3).

The exchange rate of O_2 is then integrated over the entire North Pacific north of 10°N in mode water density classes using a neutral density interval of $\Delta\gamma = 0.1$. For example, in our notation, a density bin of $\gamma = 25.6$ indicates a density range of $25.55 \leq \gamma < 25.65$. Lighter density bins ($\gamma = 24.0$–$25.5$) are referred to as the subtropical mode water (STMW) density class and denser density bins ($\gamma = 25.6$–26.6) are referred to as the central mode water (CMW) density class. The mode water density classes defined in this study are different from the classical definitions of "mode water," which is generally referred to as a water of potential vorticity less than $2 \times 10^{-10}\,\mathrm{m^{-1}\,s^{-1}}$ (Nakamura 1996; Suga et al. 1997). Thus, our STMW density class encompasses the classical "STMW" formed in the western and eastern North Pacific (Hanawa and Talley 2001). On the other hand, the CMW density class mainly forms in the central North Pacific (Fig. 5b).

3. Seasonal to decadal variability in the O_2 supply rate

The time mean transfer rate of O_2 has two peaks in two distinct density ranges, one corresponding to the STMW density class ($\gamma = 24.0$–25.5) and the other corresponding to the CMW density class ($\gamma = 25.6$–26.6) (Hanawa and Talley 2001; Fig. 6a). Annual mean O_2 subduction (Figs. 5b and 5f) mainly results from the seasonal cycle of the mixed layer depth that occurs along with horizontal migrations of surface outcrops. Shoaling of the deep winter mixed layer detrains O_2-rich surface water to the underlying thermocline during early spring (Cushman-Roisin 1987). Most seasonal subduction occurs within the winter outcrop, when its areal extent reaches a seasonal maximum (i.e., when the outcrop expands toward the equator during late winter; Figs. 5c and 5g). On the other hand, seasonal obduction occurs within outcrops whose areal extent is relatively contracted in high latitudes during fall (Figs. 5d and 5h). The imbalance between seasonal subduction rates and seasonal obduction rates leads to net annual mean O_2 subduction, which is focused within late winter (or early spring) outcrop regions (Figs. 5b and 5f; Stommel 1979). For the CMW density class, in particular, the effect of the seasonal cycle [i.e., lateral induction beneath the shoaling mixed layer base; $\int_A (-[O_2]_h Dh/Dt)\,dA$ in Eq. (3)] offsets the O_2 obduction induced by Ekman upwelling [$\int_A -[O_2]_h w_h\,dA$ in Eq. (3); Fig. 6a]. Similar to Sallée et al. (2012), we also find that mixing effects are an order of magnitude smaller than advective subduction (Fig. 6b). Thus, our focus is O_2 transport due to the subduction of water masses. Once O_2 subducts into

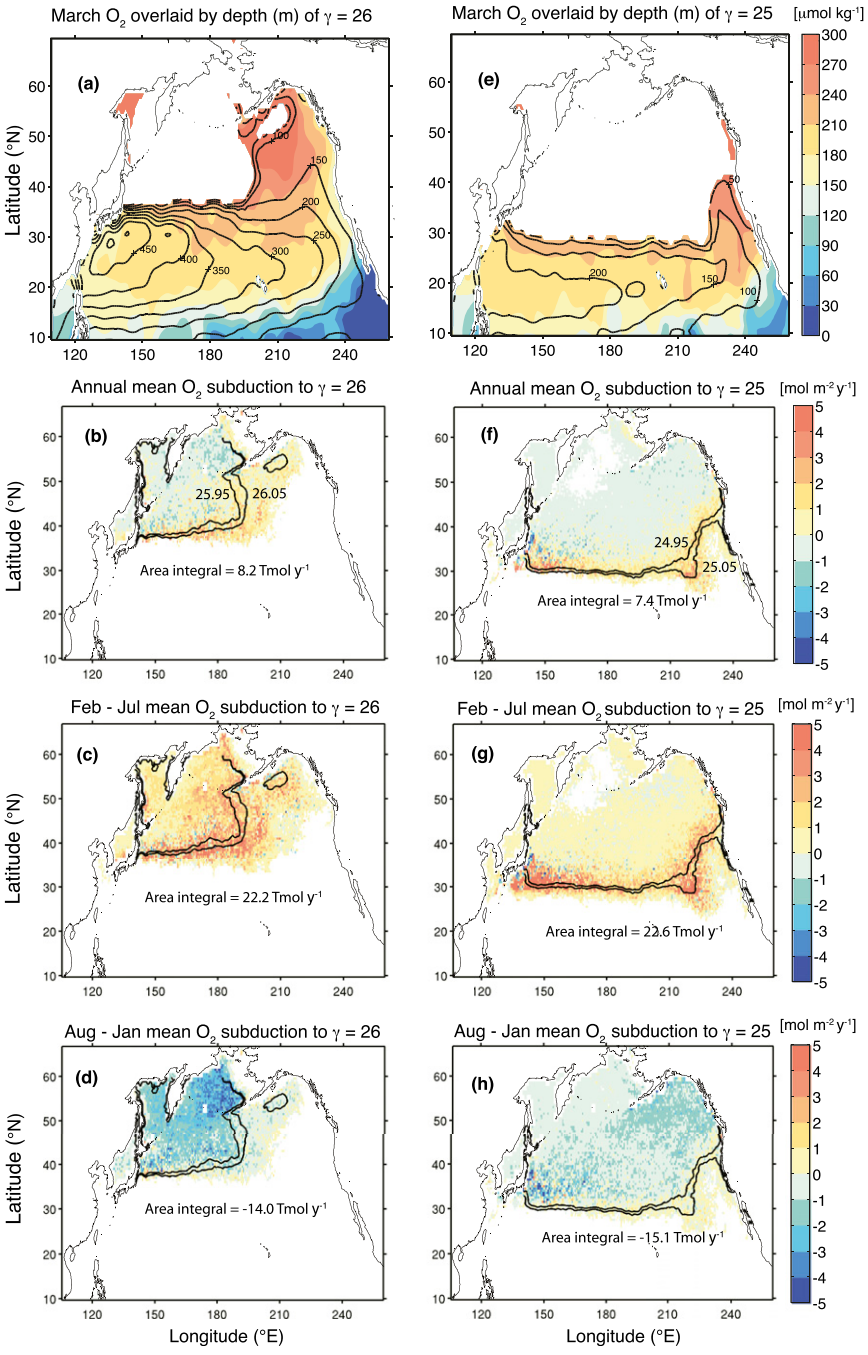

FIG. 5. The climatology of O_2 distribution and subduction on two representative isopycnal surfaces of the CMW and STMW density classes. (a) The March climatology of the O_2 distribution (μmol kg^{-1}) on a $\gamma = 26.0$ (=1026.0 kg m^{-3}) isopycnal surface, linearly interpolated from *WOA09*. The depth (m) of the isopycnal is overlain with black solid lines. White indicates the area where the isopycnal does not exist in March. (b) An annually averaged map of the O_2 subduction rate over a seasonally migrating outcrop of $\gamma = 26.0$ (mol kg^{-1} m^{-2}), an estimate from SODA and O_2 climatology data. The area integral of the subduction rate over the North Pacific is shown inside the panel using a unit of Tmol yr^{-1} (1 Tmol = 10^{12} moles). Equation (1) is integrated over 50 years for each SODA grid point in order to produce the map. Positive values represent subduction. Black contour lines represent the March outcrop of $\gamma = 26.0 \pm 0.05$ averaged from 1958 to 2007. (c) As in (b), but with the exception that the average from February to July (the subduction period) is shown. (d) As in (c), but with the exception that the average from August to January (the obduction period) is shown. (e)–(h) As in (a)–(d), but with the exception that maps for a $\gamma = 25.0$ isopycnal are shown.

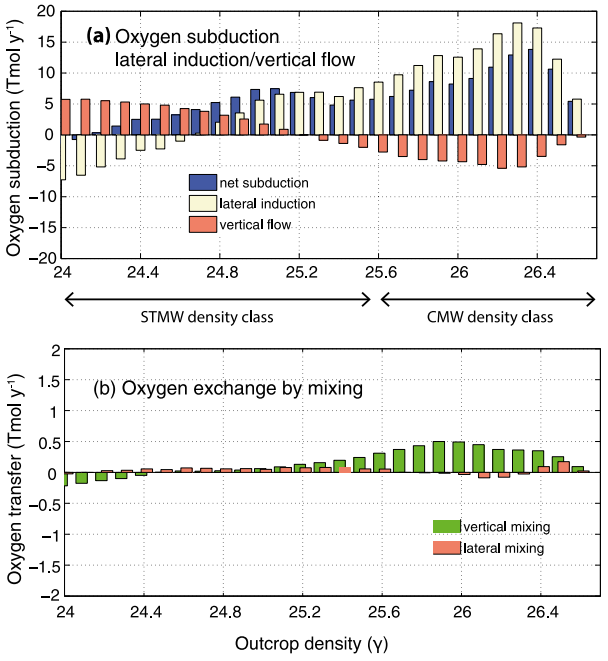

FIG. 6. The time mean subduction rate of O_2 (Tmol yr^{-1}). (a) The net subduction rate (blue) is decomposed into contributions from lateral induction beneath the shoaling mixed layer base and the vertical velocity of water at the base of the mixed layer, as expressed in Eq. (3). Positive values represent subduction (i.e., detrainment into the thermocline), and negative values represent obduction (i.e., entrainment into the mixed layer). (b) The exchange rate of O_2 due to vertical and lateral mixing, as expressed in Eq. (2). Note that the *y* scale in (b) is an order of magnitude smaller than (a). Positive values represent downward mixing into the thermocline, while negative values represent upward mixing into the mixed layer.

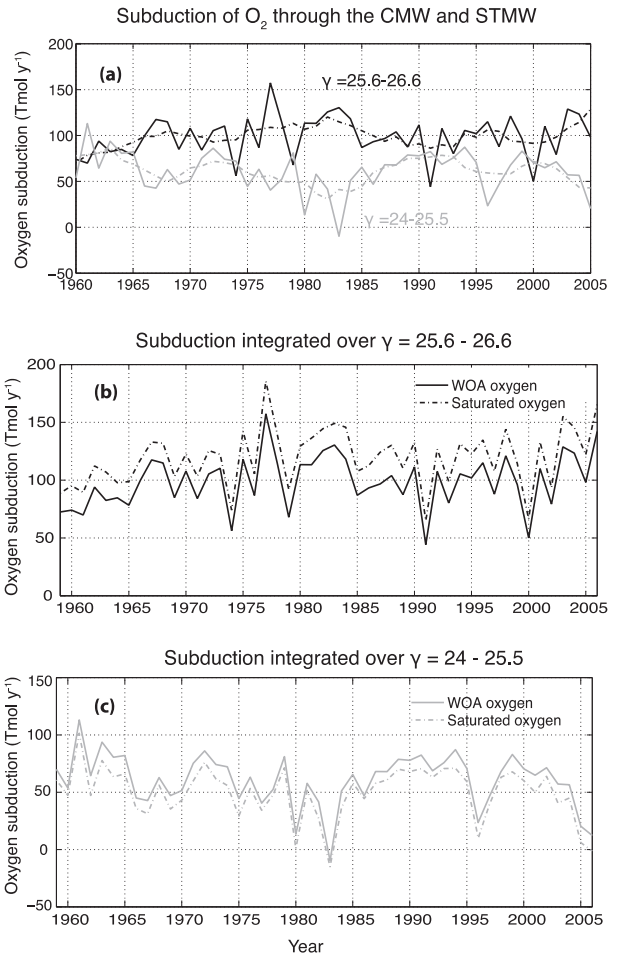

FIG. 7. Temporal variability in the annual mean O_2 subduction rate. (a) The annual mean O_2 subduction rate, integrated over the STMW density class (gray solid line) and the CMW density class (black solid line). Dashed lines are 5-yr moving averages of the corresponding time series. (b) The O_2 subduction rate to the CMW density class is obtained using *WOA09* O_2 climatology data (black solid line) and saturated O_2 estimated from SODA temperatures and salinity (black dashed line). (c) The O_2 subduction rate to the STMW density class is obtained using WOA O_2 climatology data (gray solid line) and saturated O_2 concentrations (gray dashed line). The offsets in the mean values reflect O_2 disequilibrium at the surface.

the thermocline, O_2-rich surface water spreads southward along isopycnals, and O_2 decreases as water moves away from the outcrop area (Fig. 5a and 5e).

Annual mean O_2 transfer rates integrated over the STMW and CMW density classes exhibit considerable fluctuations on interannual to decadal time scales (Fig. 7a). The time mean and standard deviations are (60 ± 23) Tmol O_2 yr^{-1} for the STMW density class and (100 ± 23) Tmol O_2 yr^{-1} for the CMW density class. Partly because of large interannual variations, we do not find any significant linear trends for the O_2 transfer rate over the past 50 years. For example, the estimated trend of -0.33 Tmol O_2 yr^{-2} for the STMW density class is smaller than the 95% confidence interval of ± 0.54 Tmol O_2 yr^{-2}. Likewise, the estimated trend of 0.36 Tmol O_2 yr^{-2} for the CMW density class is also smaller than the 95% confidence interval of ± 0.39 Tmol O_2 yr^{-2}. The lack of any significant trends is still valid even if we consider the effect of varying solubility for O_2 over the past half century (Figs. 7b and 7c). The correlation coefficients between the two estimates are above 0.98 (Figs. 7b and 7c). The strong correlations result from the fact that interannual variability in the O_2 transfer rate is dominated by variability in the water mass subduction rate rather than the variability of surface O_2 concentrations.

Multidecadal variations in O_2 subduction rates are related to the PDO, a dominant mode of climate variability in the North Pacific. Previous studies have suggested that winter mixed layer convection and stratification in the central North Pacific strongly respond to interannual variations in heat fluxes and winds at the sea surface (Qiu and Joyce 1992; Deser et al. 1996; Yasuda and

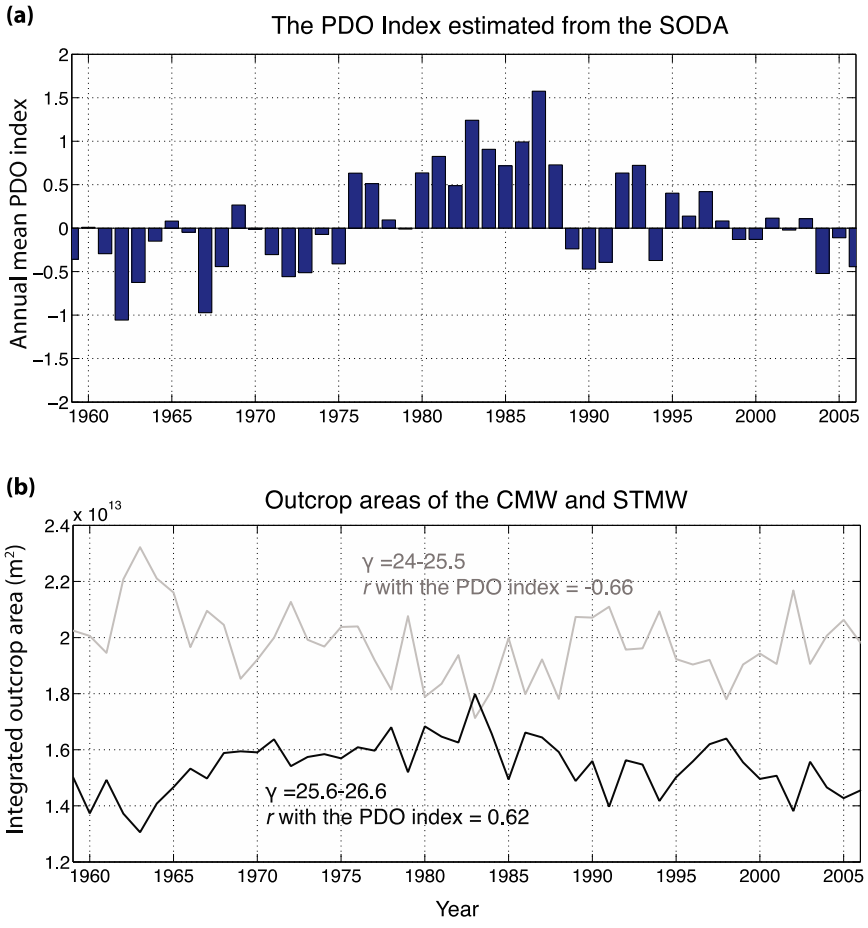

FIG. 8. (a) The annual mean PDO index estimated from SODA, the principal component time series presented in Fig. 4b. (b) March outcrop areas integrated over the CMW and STMW classes, estimates from SODA. The correlation coefficient estimated between the PDO index in (a) and the March outcrop area in (b) is $r = -0.66$ for the STMW density class (gray solid line) and $r = 0.62$ for the CMW density class (black solid line).

Hanawa 1997; Schneider et al. 1999; Xie et al. 2000). Variations in winter mixed layer depth are, in turn, accompanied by changes in the formation and subduction rates of CMW (Ladd and Thompson 2002; Qu and Chen 2009) and hence the supply rate of O_2. Figure 7a indicates that multidecadal variation in the O_2 subduction rate of the CMW density class is anticorrelated with the subduction rate of the STMW density class. Such an antiphased relationship can largely be explained through variations in outcrop areas of the CMW and STMW classes (Fig. 8b). When the central North Pacific Ocean is anomalously cold, the winter outcrop area of the CMW density water expands farther southward, resulting in a contraction of the outcrop area of the STMW density water (Schneider et al. 1999; Ladd and Thompson 2002; Oka et al. 2012; see also Figs. 3b and 8b). The expansion of the winter outcrop area of the CMW density class is associated with enhanced wintertime heat loss to the atmosphere in the central North Pacific (Fig. 3b). During positive PDO years when the CMW density outcrop is anomalously located farther south, more permanent subduction occurs because the water is unlikely to be reentrained back to the mixed layer during subsequent warm years, where the outcrop area is in its more poleward configuration. For this reason, long-term mean subduction of the CMW density class occurs south of the climatological mean outcrop locations (Fig. 5b).

To diagnose the relative importance of changes in the outcrop area, mixed layer depths, and circulation, we recompute the O_2 subduction rate after eliminating the interannual variability in each of the physical drivers, as expressed in Eqs. (4)–(6). Interannual variations in the outcrop area explain 48% of the total variance of the O_2 supply rate to the CMW density class (Fig. 9a). Interannual variations in the mixed layer depth and circulation

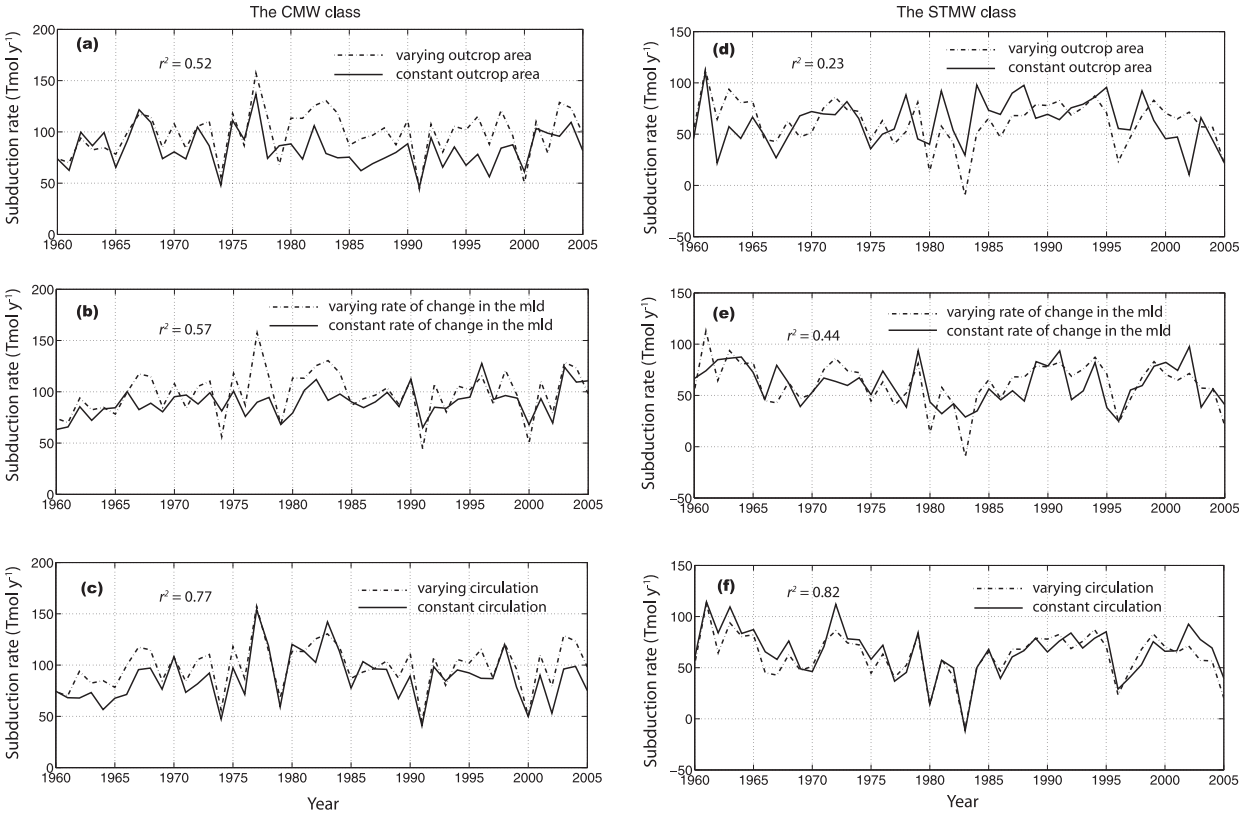

FIG. 9. The O_2 subduction rate integrated over (a)–(c) the CMW density class and (d)–(f) the STMW density class. (a),(d) The subduction rate with an interannually varying outcrop area [dashed line; M obtained using Eq. (1)] and a fixed outcrop area [solid line; M_A obtained using Eq. (4)]. (b),(e) The subduction rate with an interannually varying rate of change in the mixed layer depth (mld) [dashed line: M obtained using Eq. (1)] and a fixed rate of change in the mixed layer depth [solid line; M_h obtained using Eq. (5)]. (c),(f) The subduction rate with an interannually varying circulation [dashed line; M obtained using Eq. (1)] and a fixed circulation [solid line; M_c obtained using Eq. (6)]. The squared correlation coefficient (r^2) between the two time series, which is shown within each panel, is used to determine the explained variance by each component.

individually contribute to total variance by 43% and 23%, respectively (Figs. 9b and 9c). Interannual variations in the outcrop area also account for the highest fraction (77%) of total variance for the O_2 subduction rate to the STMW density class (Fig. 9d), followed by contributions from changes in the mixed layer depth (56%) and circulation (18%; Figs. 9e and 9f). Relative contributions from the outcrop area, the mixed layer depth, and circulation do not necessarily sum to 100% because the three factors identified are dependent on each other. For example, excess heat losses during winter tend to enhance winter mixed layer convection and at the same time expand the winter outcrop area. The combined effect leads to increased water mass formation and subduction.

The winter outcrop area correlates strongly with the PDO index ($r = 0.62$ for the CMW density class and $r = -0.66$ for the STMW density class, $p < 0.01$ for both; Figs. 8a and 8b). Since the interannual variation of the outcrop area is a primary cause of the interannnual variability of the O_2 subduction, the subduction is related to the PDO. In general, a cold phase in the central North Pacific favors an anomalously high subduction rate for O_2-rich surface water to the CMW density class. An expanded winter outcrop area, together with intensified mixed layer convection (Ladd and Thompson 2002; Qu and Chen 2009), leads to a greater amount of O_2 transferred from the mixed layer to the thermocline during the early spring in positive PDO years. On the other hand, the autumn outcrop area, over which seasonally subducted O_2 is entrained back into the mixed layer, remains fairly constant on interannual to decadal time scales. Therefore, more O_2-rich surface water can annually enter the thermocline through broader winter outcrop windows of the CMW density range during positive phases of the PDO. Such multidecadal fluctuations of the O_2 transfer rate to the CMW density class tend to be partly offset by changes in the O_2 transfer rate to the STMW density class, because the total outcrop area for both water masses is nearly conserved.

We note that significant correlations ($p < 0.05$) between the simulated PDO index (Fig. 8a) and O_2 subduction rates (Fig. 7a) are only obtained when O_2 subduction rates are smoothed using a low-pass filter. Moreover, the correlation becomes weaker than those between the outcrop area and the PDO index, because the rate of change in the mixed layer depth and ocean circulations, both are weakly correlated with the PDO index, also plays an important role in determining the interannual variability of the subduction rate (see above). Nevertheless, the fact that a low-frequency component of the O_2 subduction variability is related to the PDO is important since the thermocline circulation tends to integrate the effect of O_2 subduction on decadal time scales (Ito and Deutsch 2010). The decadal fluctuation in the O_2 uptake rates can influence multidecadal O_2 variability within the ventilated thermocline.

4. Linking subduction to observed O_2 variability

In this section, we explore the potential link between the O_2 uptake rate described in the previous section and observed O_2 variability. To this end, we use a historical dataset of O_2 concentration and discuss decadal changes in O_2 distributions on neutral density surfaces of the thermocline.

a. Mapping of O_2 data

We use quality-controlled standard-level bottle data from the World Ocean Database 2009 (WOD; available at http://www.whoi.edu/science/PO/hydrobase/php/index.php; Curry and Nobre 2013; Johnson et al. 2009; Garcia et al. 2010). After linearly interpolating discrete O_2 profiles onto neutral density surfaces (Jackett and McDougall 1997), O_2 data for each density surface are mapped onto 2° × 2° horizontal grids using Gauss–Markov mapping (Thomson and Emery 2014). In the Gauss–Markov smoothing method, the best estimate for each grid point is a linear weighted sum of neighboring observations. Weights are determined so that the mean-square error of the estimates can be minimized (Thomson and Emery 2014). For each density surface, all available data below the winter mixed layer depth are taken from a North Pacific domain of 20°–60°N, 120°–230°E, and binned into 10-yr intervals. Thus, between 1955 and 2004, five decadal mean values provide temporal changes in O_2 concentration. The mapping procedure is repeated for density surfaces of $\gamma = 25.6$–27.2, with a density interval of $\Delta\gamma = 0.1$. These density surfaces constitute the upper thermocline ventilated by subduction (section 3), as well as the lower thermocline that does not directly outcrop at the open ocean's surface. Note that O_2 variability over the STMW density class ($\gamma = 24.0$–25.5) is not considered here because decadal variability is small in the STMW density range.

Further analyses of the objectively mapped O_2 data are conducted as follows. We flag grid points where the squared mapping error exceeds 50% of observed O_2 variance within the North Pacific domain for each density surface and for each decade. For the flagged grid points, the estimation is poorly constrained due to a lack of neighboring observations or the poor quality of observed data. To reduce uncertainties in our analyses, we only consider grid points that are not flagged in any of the five decades at each density surface. This criterion excludes 20%–30% of the mapped values in the central North Pacific between 170° and 200°E, north of 36°N, and south of 28°N. We compute an O_2 anomaly relative to its climatological mean value for each grid point at each density surface (e.g., Figs. 10a–10e).

To estimate decadal changes in saturated O_2 and apparent oxygen utilization (AOU; defined as saturated O_2 concentration minus observed O_2 concentration), we use the objectively analyzed temperature and salinity data, averaged over each of the five decades between 1955 and 2004, and provided by the *World Ocean Atlas 2013* (*WOA13*; Locarnini et al. 2013; Zweng et al. 2013; available at https://www.nodc.noaa.gov/OC5/woa13/). We regrid the ¼° × ¼° *WOA13* data into 2° × 2° grids and compute saturated O_2. The *WOA13*-derived saturated O_2 data are combined with our O_2 estimate in order to compute AOU. The *WOA13* data are also used to calculate the thickness of neutral density surfaces (Figs. 11a and 11c), which are needed to compute a volume-averaged O_2 anomaly. The use of temperature and salinity obtained from the same WOD bottle data (where the O_2 data originates) does not make a discernible difference in our conclusions. Because of more extensive observations incorporated (Locarnini et al. 2013; Zweng et al. 2013), here we present results obtained using *WOA13* temperature and salinity climatologies.

b. O_2 change within the ventilated thermocline

The O_2 anomaly distribution in the CMW density range exhibits strong spatial and temporal variability (e.g., Figs. 10a–10e), reflecting complex factors determining O_2 changes within the thermocline (Deutsch et al. 2006). Despite the strong spatial dependency of O_2 variability, some features can be related to the O_2 subduction change of the CMW density. Near the winter outcrop, the thermocline tends to be better oxygenated during the 1975–84 interval (Fig. 10c), when the PDO index shifts from negative to positive. Near the winter outcrop of $\gamma = 26.0$ in the central North Pacific, O_2 anomalies are positive and up to $\sim 15\,\mu\text{mol kg}^{-1}$

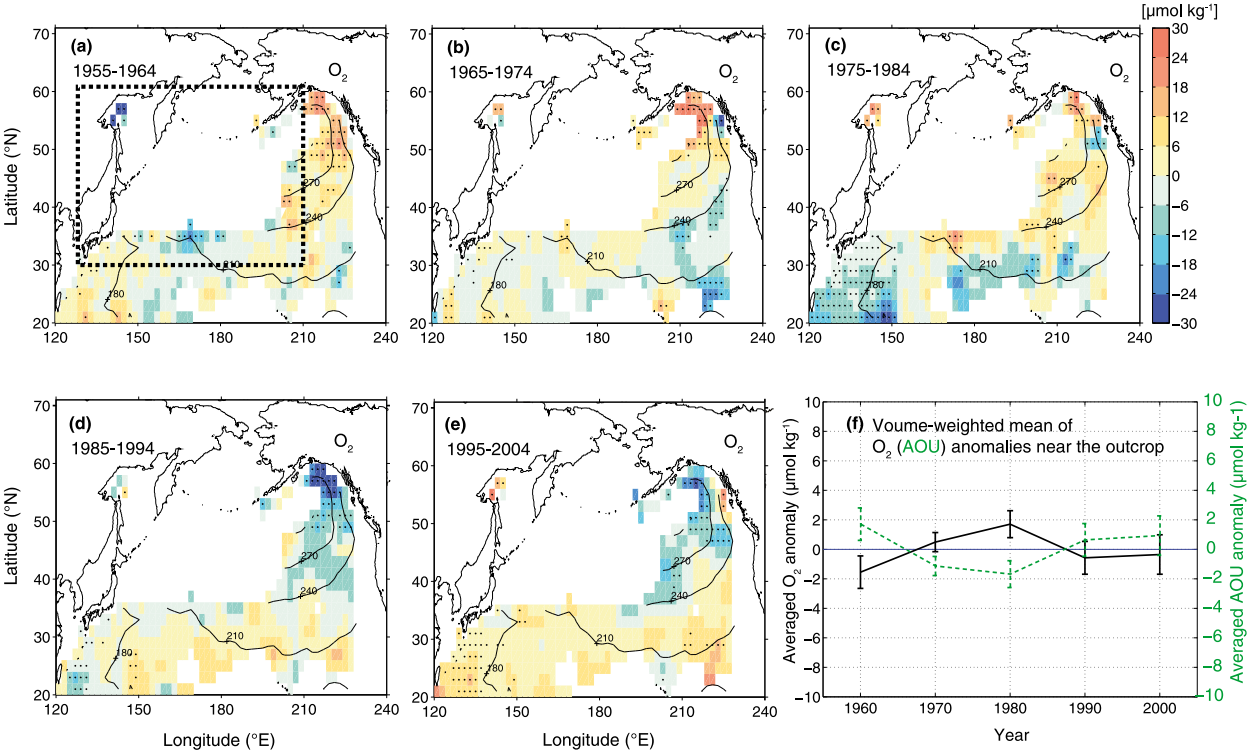

FIG. 10. Variability of O_2 anomalies on a density surface of $\gamma = 26.0$, as obtained from the World Ocean Database 2009. (a)–(e) The climatological mean distribution is shown as black solid lines. Decadal anomalies with respect to the climatological mean distribution are shown with colored shading. Values exceeding mapping errors of the corresponding grid points are marked with black dots. Decadal mean anomalies for the intervals of 1955–64, 1965–74, 1975–84, 1985–94, and 1995–2004 are presented from (a) to (e), respectively. White indicates either data gaps or the area where the isopycnal does not exist in winter. (f) Black solid line indicates the time series of the O_2 anomaly averaged over the subdomain of 30°–60°N, 120°–210°E, as shown with the dashed box in (a). The error bar takes into account mapping errors propagated through volume averaging. Green dashed line indicates the time series of the AOU anomaly averaged over the subdomain.

(approximately 7% of the climatological mean), lying above the mapping errors of the corresponding grid points.

Positive O_2 anomalies near the winter outcrop of $\gamma = 26.0$ are not caused by increasing O_2 solubility, as can be inferred from negative AOU anomalies occurring at the same time and locations. Instead, negative AOU anomalies (Fig. 10f) suggest enhanced O_2 subduction rates during the 1975–84 interval when the winter outcrop area of the CMW density class reaches its maximum (Fig. 8b). Because of the southward expansion of the winter outcrop during positive PDO years (Fig. 3b), a greater area of the thermocline can be exposed to O_2-rich surface water. This would lead to the increased area in which O_2 supply rates exceed remineralization rates. In the area near the outcrop of $\gamma = 26.0$ between 30°–60°N and 120°–210°E, the averaged O_2 anomaly peaks during the 1975–84 interval (Fig. 10f).

The period of maximum O_2 content near the winter outcrop of $\gamma = 26.0$ is followed by a period of maximum O_2 content in downstream regions of the subtropical gyre. Positive O_2 anomalies appear in most of regions south of 30°N during 1985–2004. Overall enrichments in O_2 during 1985–2004 relative to the 1975–84 period can be explained either by downstream effects of positive O_2 anomalies near the outcrop area or reduced O_2 consumption rates due to remineralization of organic matter. Considering that the ventilation time scale of the thermocline ($\sigma_\theta = 25.5$–26.6) ranges from 10 to 27 years (Sonnerup et al. 1999; Huang and Qiu 1994), a delayed downstream effect is a plausible cause. Furthermore, previous studies have suggested that North Pacific gyre circulation intensifies due to the multidecadal strengthening of the westerlies during positive PDO years (Qiu and Joyce 1992; Yasuda and Hanawa 1997; Miller et al. 1998; Deser et al. 1999; Taguchi et al. 2007). Gyre intensification would allow less O_2 to be consumed by remineralization due to a decreasing transit time from the surface (Deutsch et al. 2005, 2006).

The multidecadal trend discussed for $\gamma = 26.0$ extends throughout the entire CMW density layers ($\gamma = 25.6$–26.6), although the multidecadal change tends to be damped toward lighter density layers. In general, the

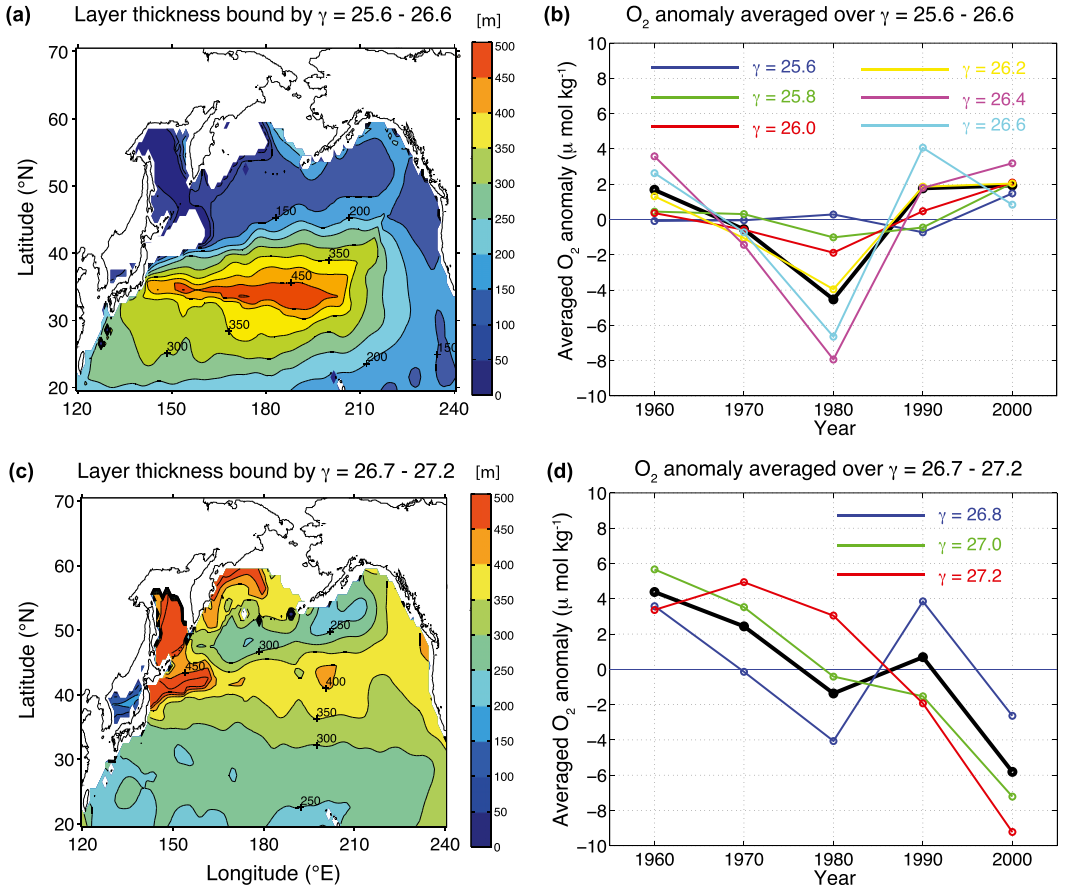

FIG. 11. (a) The thickness of the layer bounded by neutral density surfaces of $\gamma = 25.6$ and $\gamma = 26.6$, computed using the March climatology from *WOA13*. (b) Thick black solid line indicates the volume-weighted average of O_2 anomalies over the North Pacific domain of 20°–60°N, 120°–230°E within $\gamma = 25.6$–26.6. Individual averages for $\gamma =$ 25.6, 25.8, 26.0, 26.2, 26.4, and 26.6 are shown with blue, green, red, yellow, magenta, and cyan lines, respectively. (c) The thickness of the layer bounded by neutral density surfaces of $\gamma = 26.7$ and $\gamma = 27.2$. (b) Thick black solid line indicates the volume-weighted average of O_2 anomalies over the North Pacific domain of 20°–60°N, 120°–230°E within $\gamma = 26.7$–27.2. Individual averages for $\gamma = 26.8$, 27.0, and 27.2 are shown with blue, green, and red lines, respectively.

volume-averaged O_2 anomaly over the North Pacific domain from 20°–60°N, 120°–230°E displays a decreasing trend from the 1960s to the 1980s, followed by an increasing trend from the 1980s to the 2000s (Fig. 11b). In particular, the rebound from the 1980s to the 2000s is dominated by increasing O_2 within the subtropical gyre south of 30°N and is partly offset by decreasing O_2 within the Alaska gyre. The declining O_2 trend observed within the eastern subpolar gyre north of 50°N (Figs. 10d and 10e) may reflect changes in the subpolar gyre, discussed in the next section.

Reduced amplitudes of O_2 variability toward lighter densities (Fig. 11b) could arise from the compensating role of biological O_2 consumption on physically driven O_2 changes near the subtropical surface. Lighter isopycnals (e.g., $\gamma = 25.6$) outcrop near the subtropical gyre, where perennial surface nutrient depletion limits the export of organic matter and associated respiration at depth. Because of the close relationship between nutrient and O_2 cycles, changes in circulation causes O_2 supply and demand to increase at similar rates, stabilizing the overall O_2 content on density surfaces that outcrop near nutrient-limited subtropical gyres (Deutsch et al. 2006).

c. *O_2 change in intermediate water*

O_2 variability within the CMW density class contrasts with persistently declining trends in O_2 over the past 50 years, as reported for the North Pacific subpolar gyre with a density range of $\gamma = 26.7$–27.2 (e.g., Ono et al. 2001; Watanabe et al. 2003; Whitney et al. 2007; Whitney et al. 2013). The decreasing trend has been attributed

to a cessation of the winter outcrop for the isopycnal of $\sigma_\theta = 26.6$ in the latter decades of the twentieth century (Emerson et al. 2004), decreased water mass formation due to sea ice loss in the Sea of Okhotsk (Watanabe et al. 2003; Nakanowatari et al. 2007), stratification in the North Pacific subpolar gyre (Deutsch et al. 2005; 2006), and/or changes in subpolar gyre circulation and mixing (Andreev and Baturina 2006).

We define the density layer of $\gamma = 26.7$–27.2 (i.e., a density layer that does not outcrop at the open ocean surface) as the North Pacific Intermediate Water (NPIW) class, and we explore O_2 variability within the NPIW density layer. Our results confirm the declining trends in O_2 anomalies for $\gamma = 27.0$–27.2 when averaged over the North Pacific domain 20°–60°N, 120°–230°E (Fig. 11d). The decadal O_2 decline is most pronounced within the subarctic–subtropical gyre boundary (e.g., Ono et al. 2001; Emerson et al. 2004; Mecking et al. 2008), where the NPIW density water dominates (Fig. 11c). The NPIW density water forms as a mixture of the Kuroshio, Oyashio, and Tsugaru warm currents (e.g., Talley 1993), perhaps independent of direct ventilation from the surface (e.g., Qiu and Chen 2011; Yagi et al. 2014). Andreev and Baturina (2006) suggested an important role for tidal mixing within the central Aleutian and northern Kuril regions in explaining O_2 decline in the Northwest Pacific Intermediate Water. Also, it is possible that less O_2 has been replenished from the surface in source regions of the Oyashio Current, either in the Sea of Okhotsk (Nakanowatari et al. 2007) or the Bering Sea (Andreev and Watanabe 2002). The distinct formation mechanism may have led to the distinct temporal evolution of O_2 anomalies within the NPIW density class.

5. Summary

The key process by which O_2-rich mixed layer waters are transferred to the North Pacific thermocline is the subduction resulting from repeated seasonal cycles of the mixed layer depth and outcrop area. The surface outcrop window expands when the ocean takes in O_2, and it contracts when the ocean takes O_2 out of the thermocline. When averaged over the annual cycle, only a portion of seasonally subducted water is entrained back into the mixed layer during the seasonal obduction period. As a result, annual mean subduction occurs through the late winter outcrop (e.g., Figs. 5b and 5f; Stommel 1979).

The O_2 uptake rate through the base of the mixed layer is found to be sensitive to climate variations and the associated rearrangement of surface density fields. The outcrop window of North Pacific thermocline water has varied in concert with the PDO. When the central North Pacific is in a cold phase, the winter outcrop area of the CMW density class expands farther southward in the central North Pacific Ocean, allowing more O_2-rich surface water to enter the thermocline. Consistent with the decadal variations in the O_2 uptake rate, positive O_2 anomalies appear near the winter outcrop of the CMW density class during a time period of 1975–84.

The enhanced O_2 supply rate during the 1980s, combined with intensified gyre circulations (Deutsch et al. 2005, 2006), may have led to an increase in O_2 content within the ventilated thermocline of the subtropical gyre during 1985–2004. While O_2 variability within the CMW density class exhibits multidecadal fluctuations linked to the PDO, O_2 has persistently declined over the past 50 years in density layers that do not directly outcrop at the open ocean's surface (e.g., Ono et al. 2001; Emerson et al. 2004; Andreev and Baturina 2006; Whitney et al. 2007). Distinct temporal evolutions in O_2 content between the CMW density class ($\gamma = 25.6$–26.6) and the NPIW density class ($\gamma = 26.7$–27.2) suggest distinct mechanisms as the primary cause of O_2 changes.

Acknowledgments. We thank all who contributed to the compilation of the World Ocean Database. Discussions with Young Ho Kim, François Primeau, Hartmut Frenzel, and Yong-Jin Tak were very beneficial. We also thank Anand Gnanadesikan, Oleg Saenko, and three anonymous reviewers for their invaluable and constructive comments. This research was partly funded by a NRF-2013R1A1A1058203 award from the National Research Foundation of Korea. This research is also a part of the project titled "East Asian Seas Time series-I (EAST-I)," funded by the Ministry of Oceans and Fisheries, South Korea.

REFERENCES

Andreev, A. G., and S. Watanabe, 2002: Temporal changes in dissolved oxygen of the intermediate water in the subarctic North Pacific. *Geophys. Res. Lett.*, **29**, 1680, doi:10.1029/2002GL015021.

——, and V. I. Baturina, 2006: Impacts of tides and atmospheric forcing variability on dissolved oxygen in the subarctic North Pacific. *J. Geophys. Res.*, **111**, C07S10, doi:10.1029/2005JC003103.

Antonov, J. I., and Coauthors, 2010: *Salinity*. Vol. 2, World Ocean Atlas 2009, NOAA Atlas NESDIS 69, 184 pp.

Carton, J. A., and B. S. Giese, 2008: A reanalysis of ocean climate using Simple Ocean Data Assimilation (SODA). *Mon. Wea. Rev.*, **136**, 2999–3017, doi:10.1175/2007MWR1978.1.

——, G. Chepurin, X. Cao, and B. S. Giese, 2000a: A Simple Ocean Data Assimilation analysis of the global upper ocean 1950–1995. Part I: Methodology. *J. Phys. Oceanogr.*, **30**, 294–309, doi:10.1175/1520-0485(2000)030<0294:ASODAA>2.0.CO;2.

——, ——, and ——, 2000b: A Simple Ocean Data Assimilation analysis of the global upper ocean 1950–1995. Part II: Results. *J. Phys. Oceanogr.*, **30**, 311–326, doi:10.1175/1520-0485(2000)030<0311:ASODAA>2.0.CO;2.

Curry, R., and C. Nobre, 2013: Hydrobase 3. Woods Hole Oceanographic Institution Tech. Rep., 38 pp.

Cushman-Roisin, B., 1987: Subduction. *Dynamics of the Oceanic Surface Mixed Layer: Proc. 'Aha Huliko'a Hawaiian Winter Workshop*, Honolulu, HI, University of Hawai'i at Mānoa, 181–196.

de Boyer Montégut, C., G. Madec, A. S. Fischer, A. Lazar, and D. Iudicone, 2004: Mixed layer depth over the global ocean: An examination of profile data and a profile-based climatology. *J. Geophys. Res.*, **109**, C12003, doi:10.1029/2004JC002378.

Deser, C., M. A. Alexander, and M. S. Timlin, 1996: Upper-ocean thermal variations in the North Pacific during 1970–1991. *J. Climate*, **9**, 1840–1855, doi:10.1175/1520-0442(1996)009<1840:UOTVIT>2.0.CO;2.

——, ——, and ——, 1999: Evidence for a wind-driven intensification of the Kuroshio extension from the 1970s to the 1980s. *J. Climate*, **12**, 1697–1706, doi:10.1175/1520-0442(1999)012<1697:EFAWDI>2.0.CO;2.

Deutsch, C., S. Emerson, and L. Thompson, 2005: Fingerprints of climate change in North Pacific oxygen. *Geophys. Res. Lett.*, **32**, L16604, doi:10.1029/2005GL023190.

——, ——, and ——, 2006: Physical-biological interactions in North Pacific oxygen variability. *J. Geophys. Res.*, **111**, C09S90, doi:10.1029/2005JC003179.

——, A. Ferrel, B. Seibel, H.-O. Pörtner, and R. B. Huey, 2015: Climate change tightens a metabolic constraint on marine habitats. *Science*, **348**, 1132–1135, doi:10.1126/science.aaa1605.

Emerson, S., Y. W. Watanabe, T. Ono, and S. Mecking, 2004: Temporal trends in apparent oxygen utilization in the upper pycnocline of the North Pacific: 1980–2000. *J. Oceanogr.*, **60**, 139–147, doi:10.1023/B:JOCE.0000038323.62130.a0.

Garcia, H. E., R. A. Locarnini, T. P. Boyer, J. I. Antonov, O. K. Baranova, M. M. Zweng, and D. R. Johnson, 2010: Dissolved Oxygen, Apparent Oxygen Utilization, and Oxygen Saturation. Vol. 3, *World Ocean Atlas 2009*, NOAA Atlas NESDIS 70, 344 pp.

Hanawa, K., and L. D. Talley, 2001: Mode waters. *Ocean Circulation and Climate: Observing and Modelling the Global Ocean*, G. Siedler, J. Church, and J. Gould, Eds., International Geophysics Series, Vol. 77, Academic Press, 373–386.

Huang, R. X., and B. Qiu, 1994: Three-dimensional structure of the wind-driven circulation in the subtropical North Pacific. *J. Phys. Oceanogr.*, **24**, 1608–1622, doi:10.1175/1520-0485(1994)024<1608:TDSOTW>2.0.CO;2.

Ito, T., and C. Deutsch, 2010: A conceptual model for the temporal spectrum of oceanic oxygen variability. *Geophys. Res. Lett.*, **37**, L03601, doi:10.1029/2009GL041595.

Jackett, D. R., and T. J. McDougall, 1997: A neutral density variable for the world's oceans. *J. Phys. Oceanogr.*, **27**, 237–263, doi:10.1175/1520-0485(1997)027<0237:ANDVFT>2.0.CO;2.

Johnson, D. R., T. P. Boyer, H. E. Garcia, R. A. Locarnini, O. K. Baranova, and M. M. Zweng, 2009: *World Ocean Database 2009 Documentation.* NOAA Printing Office, 175 pp.

Keeling, R. F., A. Kortzinger, and N. Gruber, 2010: Ocean deoxygenation in a warming world. *Annu. Rev. Mar. Sci.*, **2**, 199–229, doi:10.1146/annurev.marine.010908.163855.

Kwon, E. Y., S. M. Downes, J. L. Sarmiento, R. Farneti, and C. Deutsch, 2013: Role of the seasonal cycle in the subduction rates of upper Southern Ocean waters. *J. Phys. Oceanogr.*, **43**, 1096–1113, doi:10.1175/JPO-D-12-060.1.

Ladd, C., and L. Thompson, 2002: Decadal variability of North Pacific central mode water. *J. Phys. Oceanogr.*, **32**, 2870–2881, doi:10.1175/1520-0485(2002)032<2870:DVONPC>2.0.CO;2.

Large, W. G., and S. G. Yeager, 2009: The global climatology of an interannually varying air-sea flux data set. *Climate Dyn.*, **33**, 341–364, doi:10.1007/s00382-008-0441-3.

——, J. McWilliams, and S. Doney, 1994: Oceanic vertical mixing: A review and a model with a nonlocal boundary layer parameterization. *Rev. Geophys.*, **32**, 363–403, doi:10.1029/94RG01872.

Locarnini, R. A., A. V. Mishonov, J. I. Antonov, T. P. Boyer, H. E. Garcia, O. K. Baranova, M. M. Zweng, and D. R. Johnson, 2010: *Temperature*. Vol. 1, World Ocean Atlas 2009, NOAA Atlas NESDIS 68, 184 pp.

——, and Coauthors, 2013: *Temperature*. Vol. 1, World Ocean Atlas 2013, NOAA Atlas NESDIS 73, 40 pp.

Mantua, N. J., S. R. Hare, Y. Zhang, J. M. Wallace, and R. C. Francis, 1997: A Pacific decadal climate oscillation with impacts on salmon. *Bull. Amer. Meteor. Soc.*, **78**, 1069–1079, doi:10.1175/1520-0477(1997)078<1069:APICOW>2.0.CO;2.

Marshall, D., 1997: Subduction of water masses in an eddying ocean. *J. Mar. Res.*, **55**, 201–222, doi:10.1357/0022240973224373.

Marshall, J. C., R. G. Williams, and A. J. G. Nurser, 1993: Inferring the subduction rate and period over the North Atlantic. *J. Phys. Oceanogr.*, **23**, 1315–1329, doi:10.1175/1520-0485(1993)023<1315:ITSRAP>2.0.CO;2.

——, D. Jamous, and J. Nilsson, 1999: Reconciling thermodynamic and dynamic methods of computation of water-mass transformation rates. *Deep-Sea Res. I*, **46**, 545–572, doi:10.1016/S0967-0637(98)00082-X.

Mecking, S., C. Langdon, R. A. Feely, C. L. Sabine, C. A. Deutsch, and D.-H. Min, 2008: Climate variability in the North Pacific thermocline diagnosed from oxygen measurements: An update based on the U.S. CLIVAR/CO_2 Repeat Hydrography cruises. *Global Biogeochem. Cycles*, **22**, GB3015, doi:10.1029/2007GB003101.

Miller, A. J., D. R. Cayan, and W. B. White, 1998: A westward-intensified decadal change in the North Pacific thermocline and gyre-scale circulation. *J. Climate*, **11**, 3112–3127, doi:10.1175/1520-0442(1998)011<3112:AWIDCI>2.0.CO;2.

Nakamura, H., 1996: A pycnostad on the bottom of the ventilated portion in the central subtropical North Pacific: Its distribution and formation. *J. Oceanogr.*, **52**, 171–188, doi:10.1007/BF02235668.

Nakanowatari, T., K. I. Ohshima, and M. Wakatsuchi, 2007: Warming and oxygen decrease of intermediate water in the northwestern North Pacific, originating from the Sea of Okhotsk, 1955–2004. *Geophys. Res. Lett.*, **34**, L04602, doi:10.1029/2006GL028243.

Nurser, A. J. G., R. Marsh, and R. G. Williams, 1999: Diagnosing water mass formation from air–sea fluxes and surface mixing. *J. Phys. Oceanogr.*, **29**, 1468–1487, doi:10.1175/1520-0485(1999)029<1468:DWMFFA>2.0.CO;2.

Oka, E., S. Kouketsu, K. Toyama, K. Uehara, T. Kobayashi, S. Hosoda, and T. Suga, 2011: Formation and subduction of central mode water based on profiling float data, 2003–08. *J. Phys. Oceanogr.*, **41**, 113–129, doi:10.1175/2010JPO4419.1.

——, B. Qiu, S. Kouketsu, K. Uehara, and T. Suga, 2012: Decadal seesaw of the Central and Subtropical Mode Water formation associated with the Kuroshio Extension variability. *J. Oceanogr.*, **68**, 355–360, doi:10.1007/s10872-011-0098-0.

Ono, T., T. Midorikawa, Y. M. Watanabe, K. Tadokoro, and T. Saino, 2001: Temporal increases of phosphate and apparent

oxygen utilization in the subsurface waters of western subarctic Pacific from 1968 to 1998. *Geophys. Res. Lett.*, **28**, 3285–3288, doi:10.1029/2001GL012948.

Qiu, B., and T. M. Joyce, 1992: Interannual variability in the mid- and low-latitude western North Pacific. *J. Phys. Oceanogr.*, **22**, 1062–1079, doi:10.1175/1520-0485(1992)022<1062:IVITMA>2.0.CO;2.

——, and S. Chen, 2011: Effect of decadal Kuroshio Extension jet and eddy variability on the modification of North Pacific Intermediate Water. *J. Phys. Oceanogr.*, **41**, 503–515, doi:10.1175/2010JPO4575.1.

Qu, T., and J. Chen, 2009: A North Pacific decadal variability in subduction rate. *Geophys. Res. Lett.*, **36**, L22602, doi:10.1029/2009GL040914.

Sallée, J.-B., R. J. Matear, S. R. Rintoul, and A. Lenton, 2012: Localized subduction of anthropogenic carbon dioxide in the Southern Hemisphere oceans. *Nat. Geosci.*, **5**, 579–584, doi:10.1038/ngeo1523.

Schneider, N., A. J. Miller, M. A. Alexander, and C. Deser, 1999: Subduction of decadal North Pacific temperature anomalies: Observations and dynamics. *J. Phys. Oceanogr.*, **29**, 1056–1070, doi:10.1175/1520-0485(1999)029<1056:SODNPT>2.0.CO;2.

Smith, R. D., J. K. Dukowicz, and R. C. Malone, 1992: Parallel ocean general circulation modeling. *Physica D*, **60**, 38–61, doi:10.1016/0167-2789(92)90225-C.

Sonnerup, R. E., P. D. Quay, and J. L. Bullister, 1999: Thermocline ventilation and oxygen utilization rates in the subtropical North Pacific based on CFC distributions during WOCE. *Deep-Sea Res. I*, **46**, 777–805, doi:10.1016/S0967-0637(98)00092-2.

Stommel, H., 1979: Determination of water mass properties of water pumped down from the Ekman layer to the geostrophic flow below. *Proc. Natl. Acad. Sci. USA*, **76**, 3051–3055, doi:10.1073/pnas.76.7.3051.

Stramma, L., A. Oschlies, and S. Schmidtko, 2012: Mismatch between observed and modeled trends in dissolved upper-ocean oxygen over the last 50 yr. *Biogeosciences*, **9**, 4045–4057, doi:10.5194/bg-9-4045-2012.

Suga, T., Y. Takei, and K. Hanawa, 1997: Thermostad distribution in the North Pacific subtropical gyre: The central mode water and the subtropical mode water. *J. Phys. Oceanogr.*, **27**, 140–152, doi:10.1175/1520-0485(1997)027<0140:TDITNP>2.0.CO;2.

——, K. Motoki, and Y. Aoki, 2004: The North Pacific climatology of winter mixed layer and mode waters. *J. Phys. Oceanogr.*, **34**, 3–22, doi:10.1175/1520-0485(2004)034<0003:TNPCOW>2.0.CO;2.

Taguchi, B., S.-P. Xie, N. Schneider, M. Nonaka, H. Sasaki, and Y. Sasai, 2007: Decadal variability of the Kuroshio Extension: Observations and an eddy-resolving model hindcast. *J. Climate*, **20**, 2357–2377, doi:10.1175/JCLI4142.1.

Talley, L. D., 1993: Distribution and formation of North Pacific Intermediate Water. *J. Phys. Oceanogr.*, **23**, 517–537, doi:10.1175/1520-0485(1993)023<0517:DAFONP>2.0.CO;2.

Thomson, R. E., and W. J. Emery, 2014: *Data Analysis Methods in Physical Oceanography*. 3rd ed. Elsevier Science, 728 pp.

Vaquer-Sunyer, R., and C. M. Duarte, 2008: Thresholds of hypoxia for marine biodiversity. *Proc. Natl. Acad. Sci. USA*, **105**, 15 452–15 457, doi:10.1073/pnas.0803833105.

Watanabe, Y. W., M. Wakita, N. Maeda, T. Ono, and T. Gamo, 2003: Synchronous bidecadal periodic changes of oxygen, phosphate and temperature between the Japan Sea deep water and the North Pacific intermediate water. *Geophys. Res. Lett.*, **30**, 2273, doi:10.1029/2003GL018338.

Whitney, F. A., H. J. Freeland, and M. Robert, 2007: Persistently declining oxygen levels in the interior waters of the eastern subarctic Pacific. *Prog. Oceanogr.*, **75**, 179–199, doi:10.1016/j.pocean.2007.08.007.

——, S. J. Bograd, and T. Ono, 2013: Nutrient enrichment of the subarctic Pacific Ocean pycnocline. *Geophys. Res. Lett.*, **40**, 2200–2205, doi:10.1002/grl.50439.

Williams, R. G., J. C. Marshall, and M. A. Spall, 1995: Does Stommel's mixed layer ''demon'' work? *J. Phys. Oceanogr.*, **25**, 3089–3102, doi:10.1175/1520-0485(1995)025<3089:DSMLW>2.0.CO;2.

Woods, J. D., and W. Barkmann, 1986: A Lagrangian mixed layer model of Atlantic 18°C water formation. *Nature*, **319**, 574–576, doi:10.1038/319574a0.

Xie, S.-P., T. Kunitani, A. Kubokawa, M. Nonaka, and S. Hosoda, 2000: Interdecadal thermocline variability in the North Pacific for 1958–1997: A GCM simulation. *J. Phys. Oceanogr.*, **30**, 2798–2813, doi:10.1175/1520-0485(2000)030<2798:ITVITN>2.0.CO;2.

Yagi, M., I. Yasuda, T. Tanaka, Y. Tanaka, K. Ono, K. I. Ohshima, and K. Katsumata, 2014: Re-evaluation of turbulent mixing vertical structure in the Bussol' Strait and its impact on water masses in the Okhotsk Sea and the North Pacific. *Prog. Oceanogr.*, **126**, 121–134, doi:10.1016/j.pocean.2014.04.023.

Yasuda, I., 2003: Hydrographic structure and variability in the Kurohsio-Oyashio transition area. *J. Oceanogr.*, **59**, 389–402, doi:10.1023/A:1025580313836.

Yasuda, T., and K. Hanawa, 1997: Decadal changes in the mode waters in the midlatitude North Pacific. *J. Phys. Oceanogr.*, **27**, 858–870, doi:10.1175/1520-0485(1997)027<0858:DCITMW>2.0.CO;2.

Zweng, M. M., and Coauthors, 2013: *Salinity*. Vol. 2, World Ocean Atlas 2013, NOAA Atlas NESDIS 74, 39 pp.